Article

Not peer-reviewed version

Interpreting Yield–Spectral Relationships in Wheat and Cotton Using a Harmonised Sentinel-2 Indicator Framework

Emmanouil Psomiadis *, Antonia Oikonomou, Marilou Avramidou, Antonis Kavvadias

Posted Date: 8 April 2026

doi: 10.20944/preprints202604.0463.v1

Keywords: crop yield; Sentinel-2; vegetation indices; precision agriculture; remote sensing; wheat; cotton

 doi:10.20944/preprints202604.0463.v1

Article

Interpreting Yield–Spectral Relationships in Wheat and Cotton Using a Harmonised Sentinel-2 Indicator Framework

Emmanouil Psomiadis *, Antonia Oikonomou, Marilou Avramidou and Antonis Kavvadias

Laboratory of Minerology and Geology, Department of Natural Resources and Agricultural Engineering, School of Environment and Agricultural Engineering, Agricultural University of Athens, 75 Iera Odos Str., Votanikos, 11855 Athens, Greece

* Correspondence: mpsomiadis@aua.gr

Abstract

Accurate estimation of crop yield from remote sensing remains challenging due to the crop-specific nature of yield drivers and the difficulty of interpreting spectral indicators across agronomic systems. While many studies prioritise predictive accuracy through complex models, fewer explicitly examine the stability and physiological relevance of individual spectral and phenological indicators under controlled analytical conditions. This study investigates yield–spectral relationships in wheat and cotton using a harmonised Sentinel-2 indicator framework applied across multiple growing seasons in a Mediterranean agricultural environment. A consistent set of spectral and thermal indicators was derived from two phenologically targeted Sentinel-2 acquisitions per season and analysed using correlation analysis, univariate regression, constrained multivariate modelling, and recurrence analysis within an identical workflow for both crops. Distinct crop-specific patterns were observed. Wheat yield was most strongly associated with water-sensitive and canopy-related indicators, with NDWI-based metrics reaching Pearson correlations up to $r = 0.85$ and multivariate models explaining a substantial proportion of yield variability (up to $R^2 \approx 0.82$) under controlled analytical conditions. In contrast, cotton yield variability was dominated by thermal accumulation, with growing degree day indicators showing correlations up to $|r| = 0.59$ and multivariate performance reaching $R^2 = 0.76$. Recurrence analysis confirmed the stability of these indicator families across analytical stages. Overall, the results indicate that parsimonious, physiologically interpretable indicator combinations can account for a substantial proportion of yield variability without reliance on black-box modelling, supporting crop-aware indicator selection for precision agriculture applications.

Keywords: crop yield; Sentinel-2; vegetation indices; precision agriculture; remote sensing; wheat; cotton

1. Introduction

Accurate estimation of crop yield remains a central objective in agricultural monitoring and precision farming, as yield integrates the cumulative effects of environmental conditions, crop physiology, and management practices throughout the growing season [1,2]. Remote sensing has become a key tool in this context, providing spatially continuous observations of crop canopies through spectral reflectance and derived vegetation indices [3,4]. These indices serve as proxies for underlying biophysical properties, such as canopy structure, chlorophyll concentration, and vegetation water status, that are directly linked to crop function and yield formation [5–7]. However, yield itself is not directly observable from space, and the relationship between spectral signals and final yield is neither linear nor universal across crops. Vegetation indices derived from multispectral satellite observations remain a key abstraction layer linking optical remote sensing data to crop biophysical processes. Indices related to canopy greenness, chlorophyll content, and vegetation water

 doi:10.20944/preprints202604.0463.v1

status provide physiologically interpretable proxies that remain widely used in yield analysis despite the increasing availability of dense time series and complex machine learning approaches [3,8–10].

A persistent challenge in satellite-based yield estimation lies in the crop-specific nature of yield drivers. Different crops respond to distinct combinations of water availability, thermal accumulation, nutrient status, and phenological timing [11–13]. Consequently, spectral indicators sensitive to particular biophysical processes may exhibit strong explanatory power for one crop or growth stage but limited relevance for another, with acquisition timing playing a critical role in determining indicator effectiveness [14]. In addition, well-documented remote sensing limitations—including index saturation at high biomass, temporal mismatches between image acquisition and critical growth stages, and strong collinearity among spectral features—complicate the interpretation of yield–spectral relationships [14,15]. These challenges highlight that yield estimation is not solely a modeling problem, but fundamentally an indicator interpretation and attribution problem, requiring an understanding of how and why specific spectral variables relate to crop performance, particularly in Mediterranean and semi-arid environments where water and thermal constraints strongly influence crop development [16].

Mediterranean agroecosystems constitute a stress-sensitive environment for yield analysis, in which crop productivity is jointly constrained by water availability, heat stress, and pronounced interannual climate variability. Under such conditions, yield responses are often non-linear and highly dependent on phenological timing, increasing the importance of indicator stability and physiological relevance [17,18]. Beyond predictive performance, understanding how individual spectral and phenological indicators relate to yield is critical for agronomic interpretation. A diagnostic perspective that examines indicator behaviour and stability under controlled analytical conditions is therefore required, particularly at the field scale [19]. Despite extensive literature on satellite-based yield estimation, many studies continue to prioritise predictive accuracy as a primary objective, often treating indicator selection as a secondary or implicit step [20–22]. High-dimensional modeling approaches are often applied directly to large sets of spectral variables without first examining the behavior, stability, or physiological relevance of individual indicators. While such approaches can improve predictive performance, they may obscure key agronomic mechanisms, particularly in small field-scale datasets typical of experimental and operational precision monitoring, where black-box optimisation may yield high apparent accuracy while masking unstable or non-physiological relationships [20,23,24]. In these contexts, indicator-level analyses, including correlation-based screening, univariate assessment, and constrained multivariate combinations, remain essential for diagnosing dominant yield drivers, identifying non-linear or saturating responses, and evaluating whether combining multiple indicators provides meaningful insight beyond single-variable relationships [25,26]. This limitation is especially relevant for operational precision agriculture, where limited sample sizes and management variability require transparent, stable, and physiologically interpretable indicators to support decision making and user trust [27,28].

Another important limitation of existing work is the lack of controlled cross-crop comparisons at the indicator level. Yield–spectral relationships are commonly investigated for individual crops using crop-specific feature sets, acquisition timings, and analytical strategies. When multiple crops are considered, differences in data structure and methodology are often confounded with crop physiology, making it difficult to isolate whether observed differences in indicator performance arise from biological processes or analytical choices [3,22,29]. In many existing studies, cross-crop comparisons implicitly involve changes in acquisition timing, indicator definitions, or modelling strategies, further complicating the interpretation of crop-specific effects [11,22,30]. As a result, empirical evidence on which spectral indicators are broadly transferable, and which are inherently crop-dependent under identical observational conditions, remains limited.

Winter cereals and summer row crops differ fundamentally in phenological timing, water-use strategies, and sensitivity to thermal stress, reflecting distinct temperature- and water-driven controls on growth and yield formation [11,31,32]. However, these physiological contrasts are rarely

 doi:10.20944/preprints202604.0463.v1

examined under identical data structures, indicator definitions, and analytical workflows, limiting the generalisation of yield–spectral relationships across crops.

To address these gaps, this study adopts a diagnostic rather than optimisation-driven perspective, investigating yield–spectral relationships in two crops with contrasting physiological characteristics—wheat and cotton—under a fully harmonised indicator framework. A consistent Sentinel-2 feature space, identical data structure, and unified analytical workflow are applied to both crops across multiple growing seasons. The analysis follows a stepwise, diagnostic approach, progressing from correlation analysis (Pearson and Spearman) to univariate regression and finally to constrained multivariate combinations. This design enables the explicit examination of the contributions and stability of individual spectral and phenological indicators before assessing whether combinations of complementary variables provide additional explanatory value.

The objective of this work is not to develop an optimised yield-prediction model, but to clarify how spectral and phenological indicators relate to yield under controlled, comparable conditions, and how these relationships differ across crops. Specifically, the study aims to (i) identify dominant crop-specific yield drivers, (ii) evaluate the stability and recurrence of spectral indicators across analytical stages, and (iii) assess the extent to which increasing indicator combinations yield additional agronomic insight. By explicitly linking indicator behaviour to crop physiology, the findings support a more interpretable and crop-aware use of remote sensing data for yield assessment and precision agriculture applications.

2. Materials and Methods

2.1. Study Area

The study was conducted at the experimental agricultural fields of the Agricultural University of Athens, located in Aliartos (38°23′41.64″ N, 23°05′55.60″ E, altitude 105 m a.s.l.), Greece (region of Viotia). The site lies within the broader Kopaida plain and is characterised by a typical Mediterranean climate, with mild to cool, relatively wet winters and warm to hot, dry summers. These climatic conditions define distinct seasonal environments for crop development and satellite-based observation across the year. The experimental site comprises 12 agricultural fields with individual areas ranging from 4.48 to 11.7 ha. Fields were cultivated with different crops during the study period according to annual crop rotation and experimental design, resulting in variation in the set of fields contributing observations across years and crops. The analysis integrated ten consecutive growing seasons, from 2016 to 2025, and included all field–year combinations for which complete yield and Sentinel-2 spectral data were available. Meteorological data used to calculate thermal indices and for climatic contextualisation were obtained from the Kopaida meteorological station operated by the Hellenic National Meteorological Service (EMY). The station is located near the experimental fields and provides representative temperature measurements for the study area. The two crops analysed represent contrasting agronomic systems within the same geographical setting. Wheat was cultivated as a winter cereal, with canopy development occurring primarily during the cooler part of the year, while cotton was cultivated as a summer row crop, developing under warmer seasonal conditions. These differences result in distinct phenological windows and acquisition periods for satellite observations while maintaining a consistent spatial and climatic context.

 doi:10.20944/preprints202604.0463.v1

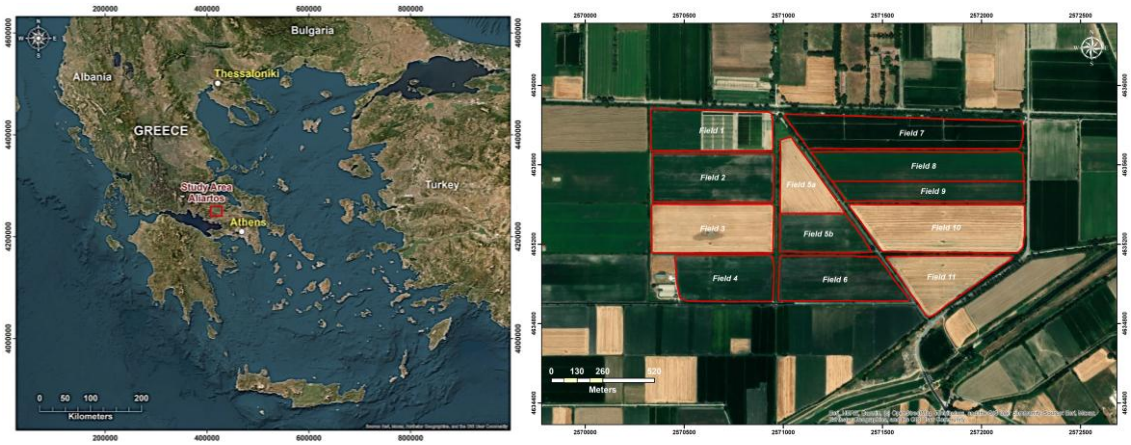

(**a**) (**b**)

Figure 1. Location and layout of the Agricultural University of Athens experimental fields in Aliartos, Greece. (a) Geographic location of the study area. (b) High-resolution satellite image showing the boundaries and identifiers of the experimental agricultural fields used in the study. Fields were cultivated with different crops across years according to the experimental design.

2.2. Study Design and Analytical Framework

The modeling framework focused exclusively on spectral and phenological indicators. Soil characteristics and management variables (e.g., fertilization, irrigation, tillage) were not explicitly included in the models. The experimental area is managed using consistent, uniform conventional agronomic practices, with no major management changes throughout the study period. The methodological design of this study follows a stepwise, interpretable analytical framework applied identically to both wheat and cotton to enable direct comparison. The analysis progressively examines yield–spectral relationships through correlation analysis, univariate regression, and constrained multivariate modelling. This structure allows the explicit evaluation of the contributions of individual spectral and phenological indicators before assessing the added value of combining complementary predictors (Figure 2).

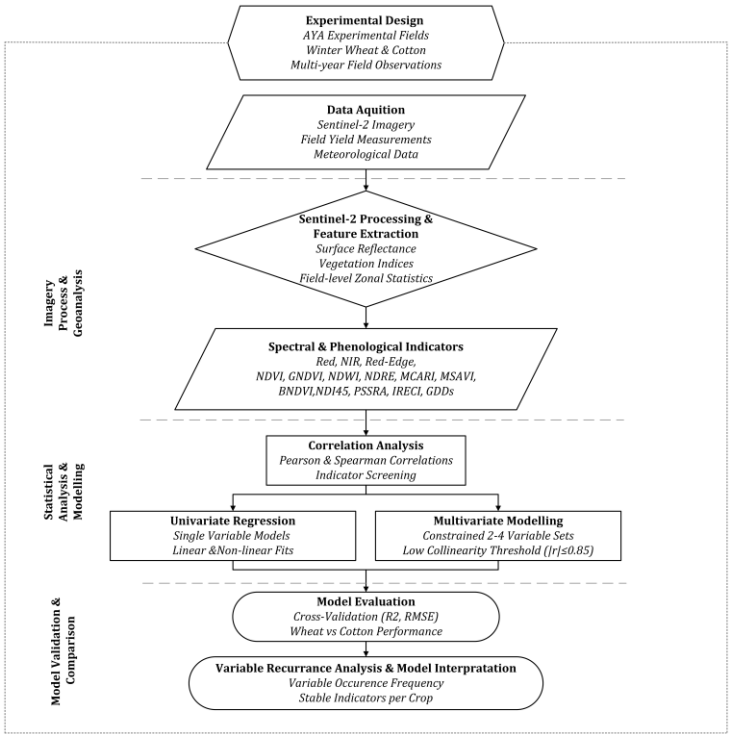

Figure 2. Study Design and Framework flowchart.

 doi:10.20944/preprints202604.0463.v1

All analyses were performed separately for each crop but used the same data structure, feature space, and analytical workflow. Sentinel-2 imagery was processed and pre-processed using ESA SNAP (v. 12.0.0), and all spectral bands and vegetation indices were derived consistently from surface reflectance products following a unified processing chain. Field-level spectral variables were extracted using zonal statistics (e.g., mean reflectance and index values per field polygon) implemented in ArcGIS Pro (v. 3.6.0). The statistical analyses and modelling workflow, including correlation analysis and regression model evaluation, were implemented in a single reproducible modelling environment (Python v. 3.11.9), ensuring that observed differences in yield–spectral relationships could be attributed to crop-specific characteristics rather than methodological inconsistencies. All analyses were executed using standard scientific Python libraries for data handling and modelling. Emphasis was placed on interpretability and agronomic relevance rather than on maximising predictive accuracy through complex black-box approaches, reflecting the study's limited sample size and the precision agriculture context in which it was applied.

2.3. Dataset Structure and Yield Observations

The analytical dataset was organised at the field–year level, with each record corresponding to one agricultural field monitored during a single growing season. Final measured yield, expressed in kilograms per stremma, was available for all records and served as the dependent variable throughout the analysis.

The study covered ten growing seasons (2016–2025) and included all field–year combinations for which complete yield and spectral data were available. Due to annual crop rotation and experimental planning, not all fields were cultivated with the same crop each year. Consequently, the set of fields contributing observations varied across seasons and crops, resulting in different numbers of field–year entries for wheat and cotton. So, some fields contribute observations in multiple years, depending on crop rotation.

The wheat dataset comprised 27 field–year observations, while the cotton dataset comprised 33. Despite differences in sample size, the two datasets shared the same predictor structure. All spectral, phenological, and derived variables were defined consistently across crops, with differences arising solely from crop-specific satellite image acquisition timing. Across the analysed field–year observations, wheat yields ranged from approximately 80 to 570 kg stremma^{-1} (mean ± SD: 418 ± 133 kg stremma^{-1}), while cotton yields ranged from approximately 350 to 585 kg stremma^{-1} (mean ± SD: 468 ± 60 kg stremma^{-1}). These ranges provide context for interpreting the magnitude of reported RMSE values.

A total of 47 predictor variables (excluding identifiers and target variable) were included for each field–year record, comprising raw spectral bands, vegetation indices, phenological variables, and temporal or composite metrics. The complete list of variables and their definitions is provided in Table 1. Squared vegetation index terms (e.g., NDVI2_SQ) were included to capture known non-linear and saturating canopy–yield responses, particularly under dense or late-season canopy conditions where linear NDVI sensitivity diminishes (Figure 3).

Table 1. Predictor variables used in the analysis, grouped by variable family with corresponding spectral definitions.

Variable family	Variables	Description	Equation / spectral definition
Identification	YEAR, FIELD	Crop season and field identifier	–
Temporal metrics	Ddays	Days between Sentinel-2 acquisitions	$Ddays = Date_2 - Date_1$
Thermal metrics	GDD1, GDD2, GDD_DIFF	Thermal accumulation and	$GDD = \Sigma \max(0, Tmean - Tbase)$[33]; $GDD\_DIFF = GDD2 - GDD1$

 doi:10.20944/preprints202604.0463.v1

		inter-date progression	
Raw spectral bands	RED(1–2), NIR(1–2), RE3(1–2)	Red, near-infrared, and red-edge reflectance	RED = B4 (665 nm); NIR = B8 (842 nm); RE3 = B7 (783 nm)
NDVI family	NDVI(1–2), NDVI_DIFF, NDVI_RATE, NDVI_MEAN, NDVI2_SQ	Canopy greenness and temporal NDVI metrics	NDVI = (NIR − RED) / (NIR + RED)[34]; NDVI_DIFF = NDVI2 − NDVI1; NDVI_RATE = (NDVI2 − NDVI1) / Ddays; NDVI_MEAN = (NDVI1 + NDVI2)/2; NDVI2_SQ = $(NDVI2)^2$
GNDVI family	GNDVI(1–2), GNDVI_DIFF, GNDVI_RATE	Chlorophyll-sensitive greenness indices	GNDVI = (NIR − GREEN) / (NIR + GREEN)[35]
NDWI family	NDWI(1–2), NDWI_DIFF, NDWI_RATE, NDWI_MEAN	Vegetation water status indices	NDWI = (NIR − SWIR) / (NIR + SWIR)[36]; NDWI_DIFF = NDWI2 − NDWI1; NDWI_RATE = (NDWI2 − NDWI1) / Ddays; NDWI_MEAN = (NDWI1 + NDWI2)/2
Red-edge indices	NDRE(1–2), IRECI(1–2)	Red-edge chlorophyll sensitivity	NDRE = (NIR − RE3) / (NIR + RE3)[37]; IRECI = (NIR − RED) / (RE3 / RE2)[38]
Pigment indices	MCARI(1–2), PSSRA(1–2)	Chlorophyll and pigment-related indices	MCARI = [(RE3 − RED) − 0.2(RE3 − GREEN)]·(RE3 / RED)[39]; PSSRA = NIR / RED[40]
Soil-adjusted indices	MSAVI(1–2), BNDVI(1–2)	Soil background-adjusted vegetation indices	MSAVI = (2·NIR + 1 − $\sqrt{}$((2·NIR + 1)² − 8·(NIR − RED))) / 2 [41]; BNDVI = (NIR − BLUE) / (NIR + BLUE) [42]
Normalised difference indices	NDI45(1–2)	Green–red contrast indices	NDI45 = (RE − RED) / (RE + RED) [43]
Inter-date band changes	RED_DIFF, RE3_DIFF, NIR_DIFF	Spectral change between acquisitions	$Band\_DIFF = Band_2 - Band_1$
Composite metrics	NDVI_RATIO, NDVIxNDWI, MCARIxNDRE	Ratio and interaction terms	NDVI_RATIO = NDVI2 / NDVI1; NDVIxNDWI = NDVI2 · NDWI2; MCARIxNDRE = MCARI2 · NDRE2
Target variable	YIELD	Final measured yield	kg $stremma^{-1}$

Note: Subscripts (1) and (2) denote the first and second Sentinel-2 image acquisitions selected within each growing season, respectively. Variables with subscript 1 correspond to indicators calculated from the earlier acquisition date, while variables with subscript 2 correspond to indicators calculated from the later acquisition date. Inter-date metrics (e.g., _DIFF, _RATE, _MEAN, _RATIO) were derived using values from both acquisitions as specified in the corresponding equations.

 doi:10.20944/preprints202604.0463.v1

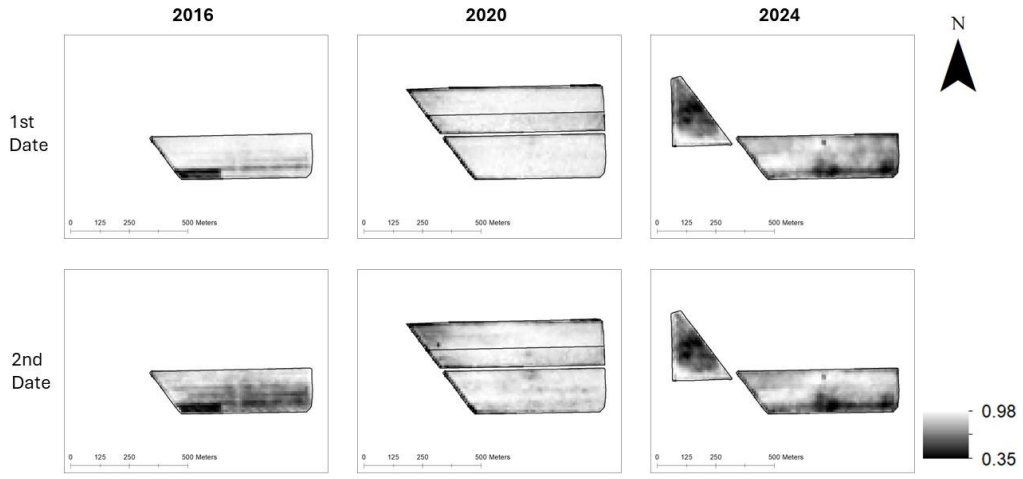

Figure 3. Spatial distribution of NDVI in a wheat field for the years 2016, 2020, and 2024, shown for two acquisition dates (late April and early May) to illustrate intra-seasonal variability in crop vigor.

2.4. Sentinel-2 Data and Spectral Feature Derivation

Satellite observations were derived from the Copernicus Sentinel-2 mission, which comprises two identical satellites in the same orbit. Each satellite carries an innovative wide-swath, high-resolution multispectral imager with 13 spectral bands, providing a new perspective on land and vegetation. The Sentinel-2 Level-2A multispectral imagery provides atmospherically corrected surface reflectance data. For each growing season and crop, two cloud-free acquisitions were selected to represent phenologically meaningful stages relevant to yield formation. Acquisition dates were selected to capture key phases of canopy development for each crop, corresponding to periods of active vegetative growth and physiological differentiation, while maintaining consistency across seasons and minimizing cloud contamination. (Table 2).

The use of two phenologically targeted Sentinel-2 acquisitions per growing season represents a deliberate methodological choice. This design prioritises interpretability and controlled comparison across crops while limiting model complexity given the available sample size. Rather than relying on dense time-series metrics or seasonal integrals, which introduce additional modelling assumptions and data requirements, the selected approach focuses on physiologically meaningful indicators that capture canopy status and change across key developmental stages.

Mean reflectance values were extracted at the field-polygon level and used to compute a comprehensive set of spectral variables. These included raw reflectance bands in the red, near-infrared, and red-edge regions, as well as vegetation indices representing canopy greenness, chlorophyll and pigment sensitivity, vegetation water status, and soil-adjusted canopy structure. To capture intra-seasonal crop dynamics, additional derived metrics were calculated between the two acquisition dates, including inter-date differences, rates of change, ratios, and interaction terms. All spectral variables were computed using standard formulations and aggregated at the field level.

Table 2. Complete list of Sentinel-2 images used.

Image	Date	Image	Date
S2A_MSIL2A_20160424T092032_N0500_R093_T34SFH_20231024T025104	24/04/2016	S2A_MSIL2A_20160822T092032_N0500_R093_T34SFH_20231019T120119	22/08/2016
S2A_MSIL2A_20160514T092032_N0500_R093_T34SFH_20231004T193729	14/05/2016	S2A_MSIL2A_20160901T092032_N0500_R093_T34SFH_20231024T071005	01/09/2016
S2A_MSIL2A_20170429T092031_N0500_R093_T34SFH_20230923T194201	29/04/2017	S2B_MSIL2A_20170829T090549_N0500_R050_T34SFH_20231016T034804	29/08/2017
S2B_MSIL2A_20170511T091019_N0500_R050_T34SFH_20231112T043851	11/05/2017	S2B_MSIL2A_20170908T091019_N0500_R050_T34SFH_20230929T093341	08/09/2017
S2B_MSIL2A_20180429T092029_N0500_R093_T34SFH_20230804T180939	29/04/2018	S2B_MSIL2A_20180827T092019_N0500_R093_T34SFH_20230806T055451	27/08/2018

 doi:10.20944/preprints202604.0463.v1

S2A_MSIL2A_20180514T092031_N0500_R093_T34SFH_20230903T203819	14/05/2018	S2A_MSIL2A_20180908T090551_N0500_R050_T34SFH_20230804T112520	08/09/2018
S2A_MSIL2A_20190429T092031_N0500_R093_T34SFH_20221024T095607	29/04/2019	S2A_MSIL2A_20190824T090601_N0500_R050_T34SFH_20230720T153109	24/08/2019
S2B_MSIL2A_20190511T090559_N0500_R050_T34SFH_20221211T020507	11/05/2019	S2A_MSIL2A_20190906T092031_N0500_R093_T34SFH_20230627T235111	06/09/2019
S2B_MSIL2A_20200428T092029_N0500_R093_T34SFH_20230419T214056	28/04/2020	S2B_MSIL2A_20200823T090559_N0500_R050_T34SFH_20230519T201544	23/08/2020
S2A_MSIL2A_20200513T092031_N0500_R093_T34SFH_20230427T202650	13/05/2020	S2B_MSIL2A_20200902T090559_N0500_R050_T34SFH_20230426T234536	02/09/2020
S2B_MSIL2A_20210430T090549_N0500_R050_T34SFH_20230311T202449	30/04/2021	S2A_MSIL2A_20210823T090601_N0500_R050_T34SFH_20230217T170707	23/08/2021
S2B_MSIL2A_20210513T092029_N0500_R093_T34SFH_20230330T145005	13/05/2021	S2A_MSIL2A_20210902T090601_N0500_R050_T34SFH_20230114T090404	02/09/2021
S2B_MSIL2A_20220428T092019_N0510_R093_T34SFH_20240610T125012	28/04/2022	S2A_MSIL2A_20220831T091611_N0510_R093_T34SFH_20240703T111010	31/08/2022
S2B_MSIL2A_20220515T090559_N0510_R050_T34SFH_20240619T065522	15/05/2022	S2A_MSIL2A_20220910T091601_N0510_R093_T34SFH_20240727T020443	10/09/2022
S2A_MSIL2A_20230428T092031_N0510_R093_T34SFH_20240831T182132	28/04/2023	S2B_MSIL2A_20230831T091559_N0510_R093_T34SFH_20241017T232234	31/08/2023
S2A_MSIL2A_20230518T092031_N0510_R093_T34SFH_20240905T194404	18/05/2023	S2A_MSIL2A_20230912T090601_N0510_R050_T34SFH_20240825T094904	12/09/2023
S2B_MSIL2A_20240427T091549_N0510_R093_T34SFH_20240427T105531	27/04/2024	S2B_MSIL2A_20240825T091549_N0511_R093_T34SFH_20240826T145644	25/08/2024
S2A_MSIL2A_20240519T090601_N0510_R050_T34SFH_20240519T154047	19/05/2024	S2A_MSIL2A_20240909T092031_N0511_R093_T34SFH_20240909T141649	09/09/2024
S2A_MSIL2A_20250426T091321_N0511_R050_T34SFH_20250426T122912	26/04/2025	S2C_MSIL2A_20250825T092051_N0511_R093_T34SFH_20250825T125221	25/08/2025
S2A_MSIL2A_20250519T092041_N0511_R093_T34SFH_20250519T125816	19/05/2025	S2A_MSIL2A_20250906T092231_N0511_R093_T34SFH_20250906T130312	06/09/2025

2.5. Phenological and Thermal Variables

Crop phenological development was characterised using Growing Degree Days (GDD) accumulated from the start of each growing season up to each Sentinel-2 acquisition date. Both the accumulated GDD values at each acquisition and the inter-date difference were included to represent thermal progression within the growing season.

These variables were incorporated to provide phenological context to the spectral observations and to account for crop-specific sensitivity to thermal accumulation. This representation is particularly relevant for cotton, whose yield formation is strongly influenced by cumulative heat exposure during the growing period.

2.6. Data Pre-processing and Quality Control

All variables were examined prior to analysis to ensure data integrity and internal consistency. Spectral variables were extracted as field-level means from Sentinel-2 imagery; therefore, no additional spatial aggregation was required. The dataset was screened for missing values and implausible entries, and only complete field–year records were retained for analysis. No data imputation was applied. Variables used solely for identification, such as year and field code, were excluded from all modelling steps.

Predictor variables were retained in their original physical units and index formulations. No explicit standardisation or normalisation was applied, as the analysis prioritised the interpretability of indicator behaviour and included regression model families (e.g., tree-based methods) that are insensitive to variable scaling. Model evaluation relied on cross-validation rather than absolute coefficient magnitudes.

Before multivariate modelling, the correlation structure among predictors was examined as a diagnostic step to assess redundancy and potential multicollinearity among spectral, phenological, and derived variables. Pairwise correlation analysis was used to identify highly correlated variable pairs, informing the constrained predictor selection applied in subsequent multivariate modelling. No automated dimensionality reduction or feature elimination was performed at this stage.

 doi:10.20944/preprints202604.0463.v1

2.7. Correlation Analysis

Correlation analysis was performed using both Pearson's correlation coefficient and Spearman's rank correlation coefficient to characterise the relationship between yield and all spectral, phenological, and derived variables. Pearson correlation was used to quantify linear associations, while Spearman correlation was employed to assess monotonic relationships and provide robustness against non-normal distributions and potential outliers.

Correlation matrices were computed separately for wheat and cotton to quantify the strength and direction of yield–indicator relationships, identify crop-specific correlation patterns, and evaluate collinearity among predictors. Correlation heatmaps and ranked correlation tables derived from both sets of coefficients were used for exploratory and diagnostic purposes, and to guide the interpretation and selection of variables in subsequent regression analyses. Correlation analysis was used as a comparative and diagnostic tool rather than as a formal hypothesis-testing framework.

2.8. Univariate Regression Analysis

Univariate regression analysis was conducted to quantify the individual explanatory power of each predictor for yield. For each spectral and phenological variable, regression models were fitted independently, without including additional covariates or interaction terms.

Model performance was evaluated using repeated k-fold cross-validation to ensure robustness given the limited sample size. Specifically, a 5-fold cross-validation, repeated three (3) times, was applied; models were trained on 4 folds and evaluated on the remaining fold, with all folds and repetitions iteratively cycled. Cross-validation splits were generated using a fixed random seed to ensure reproducibility across modeling runs. The coefficient of determination (R^2) reported for each univariate model corresponds to the mean cross-validated R^2 across all folds and repetitions.

For each predictor, multiple functional forms were evaluated, including linear and quadratic terms, to capture potential nonlinear or saturating responses. For each variable, the regression method and functional form yielding the highest mean cross-validated R^2 were retained. This analysis constituted a core step, enabling the identification of dominant individual indicators, the assessment of non-linear behavior, and the comparison of indicator performance across crops under identical analytical conditions, free from multicollinearity.

2.9. Constrained Multivariate Yield Modeling

Building on the univariate results, constrained multivariate regression models were developed to assess whether combinations of complementary predictors improved the explanatory power of yield beyond single-indicator models. Multivariate modeling was intentionally restricted to preserve interpretability and to limit overfitting, given the relatively small sample size.

Multivariate models were limited to a small number of predictors (two to four per model). Candidate predictor combinations were generated under a pragmatic low-collinearity constraint, whereby no pair of variables within the same model was allowed to exceed a pairwise Pearson correlation of $|r| = 0.85$. This relatively conservative threshold was selected to exclude severe redundancy while preserving physiologically related spectral indicators that commonly exhibit moderate correlation in multispectral vegetation index spaces.

Model performance was evaluated using the same repeated 5-fold cross-validation scheme (three repeats) applied in the univariate analysis, ensuring consistency in performance assessment across modeling stages. Using an identical cross-validation strategy and evaluation metric across the univariate and multivariate stages ensured that model performance comparisons reflected differences in predictor structure rather than differences in the evaluation procedure. Predictor combinations were further guided by strong univariate performance and by the representation of distinct physiological processes, such as canopy structure, vegetation water status, and phenological development. Separate sets of multivariate models were developed for wheat and cotton using

 doi:10.20944/preprints202604.0463.v1

identical selection criteria and modeling logic. The regression model families evaluated at each analytical stage are summarised in Table 3.

Cross-validation splits were generated randomly at the field–year level rather than blocked by year or by field. As a result, observations from different years in the same field may appear in both the training and testing folds, potentially introducing partial temporal dependence, particularly for climate-driven predictors such as growing degree days. Consequently, reported performance metrics should be interpreted as upper-bound estimates of explanatory consistency rather than conservative measures of predictive generalisation.

Table 3. List of models used.

Analysis stage	Model type	Regression methods	Predictor setup
Univariate / Multivariate	Linear	Ordinary Least Squares (OLS), Ridge, Lasso, ARD, Huber	Single predictor / 2-4 predictors
	Non-linear	Random Forest, ExtraTrees, AdaBoost	Single predictor / 2-4 predictors

3. Results

3.1. Yield–Spectral Correlation Patterns

Table 4 summarises the strongest correlations between yield and selected input variables for wheat and cotton, based on Pearson's correlation coefficient, together with the corresponding Spearman rank correlations. Among wheat variables, the five with the highest absolute Pearson correlations with yield are NDWI_MEAN, NDWI1, MSAVI1, NDWI2, and NDVI_MEAN. Pearson correlation coefficients for these variables range from 0.778 to 0.848, whereas Spearman correlation coefficients range from 0.688 to 0.774.

For cotton, the five variables with the highest absolute Pearson correlation with yield are GDD_DIFF, GDD2, RED2, NDI452, and NDVI2. Pearson correlation coefficients for these variables range from 0.448 to 0.588 in absolute value, whereas Spearman correlation coefficients range from 0.433 to 0.632. Correlation results are reported separately for each crop and are presented in full in Table 4.

Table 4. Strongest correlations between yield and input variables for wheat and cotton.

Crop	Variable	Pearson r	Spearman ϱ
Wheat	NDWI_MEAN	0.848	0.715
	NDWI1	0.835	0.707
	MSAVI1	0.819	0.774
	NDWI2	0.804	0.703
	NDVI_MEAN	0.778	0.688
Cotton	GDD_DIFF	−0.588	−0.632
	GDD2	−0.495	−0.433
	RED2	−0.484	−0.535
	NDI452	0.455	0.520
	NDVI2	0.448	0.452

3.2. Univariate Regression Results

Table 5 presents the highest-performing univariate regression model configurations for wheat and cotton, evaluated using the coefficient of determination (R^2). Multiple regression methods were tested for each predictor, and Table 5 reports the top-performing variable–model combinations based on R^2.

 doi:10.20944/preprints202604.0463.v1

For wheat, the highest univariate R^2 was achieved using GDD1 with an ExtraTrees regressor (R^2 = 0.755). In addition, several linear model configurations using NDWI-based variables show strong performance, including OLS, ARD, Huber, and Lasso regressions applied to NDWI_MEAN and NDWI1, with R^2 values ranging from 0.637 to 0.672.

For cotton, the strongest univariate models are dominated by thermal variables. The highest R^2 values are obtained using Random Forest regressors with GDD_DIFF (R^2 = 0.439), GDD1 (R^2 = 0.431), and GDD2 (R^2 = 0.401). Additional univariate models using alternative regression methods, including ExtraTrees, AdaBoost, and Ridge regression, are also reported in Table 5. Corresponding root mean square error (RMSE) values for all listed models are provided alongside R^2 and are expressed in kilograms per stremma (kg stremma^{-1}).

Table 5. Best-performing univariate yield models for wheat and cotton.

Crop	Variable	Model	R^2	RMSE
Wheat	GDD1	ExtraTrees	0.755	62.27
	NDWI_MEAN	OLS	0.672	72.05
	NDWI1	OLS	0.650	74.40
	NDWI_MEAN	ARD	0.670	72.26
	NDWI_MEAN	Huber	0.664	72.89
	NDWI_MEAN	Lasso	0.662	73.06
	NDWI1	OLS	0.650	74.40
	NDWI1	ARD	0.649	74.54
	NDWI1	Lasso	0.644	75.02
	NDWI1	Huber	0.637	75.77
Cotton	GDD_DIFF	RandomForest	0.439	45.38
	GDD1	RandomForest	0.431	45.73
	GDD_DIFF	AdaBoost	0.430	45.76
	GDD2	RandomForest	0.401	46.92
	GDD1	ExtraTrees	0.391	47.31
	GDD_DIFF	ExtraTrees	0.387	47.45
	GDD2	ExtraTrees	0.376	47.88
	GDD2	AdaBoost	0.365	48.31
	GDD1	AdaBoost	0.356	48.63

3.3. Constrained Multivariate Modeling Results

Tables 6 and 7 summarise the highest-performing constrained multivariate models for wheat and cotton, respectively. For wheat, multivariate models included between three and four predictors and achieved R^2 values ranging from 0.803 to 0.824. The top-performing wheat model combined NDWI2, NIR_DIFF, NDI451, and BNDVI1 using an ordinary least squares (OLS) regression, achieving an R^2 of 0.824 and an RMSE of 52.80 kg stremma^{-1}. Across the highest-ranked wheat models, NDWI2 and inter-date canopy change metrics (NIR_DIFF, RE3_DIFF) are consistently present, whereas alternative linear estimators (OLS, Huber, and ARD) achieve comparable performance under the constrained-predictor setup. Additional high-performing wheat models and their corresponding RMSE values are reported in Table 6.

For cotton, constrained multivariate models included between two and four predictors and achieved R^2 values ranging from 0.738 to 0.758. The highest-performing cotton models were obtained using ExtraTrees regressors combining thermal and spectral variables. Top-ranked configurations include a three-variable model combining GDD1, NDVI2_SQ, and RED1, as well as a parsimonious two-variable model combining GDD_DIFF and NDVI_MEAN, both achieving an R^2 of 0.758 with an RMSE of 29.79 kg stremma^{-1}. Across the reported cotton models, thermal accumulation metrics (GDD1, GDD2, GDD_DIFF) recur alongside canopy condition indicators, confirming the

 doi:10.20944/preprints202604.0463.v1

complementary role of spectral information once phenological timing is accounted for. All reported multivariate cotton models and their associated performance metrics are listed in Table 7.

Given the limited number of fields–year observations available for both crops, absolute performance metrics should be interpreted cautiously. The objective of the constrained multivariate analysis is not to establish transferable predictive models, but to assess the relative explanatory contribution and recurrence of indicator families under controlled analytical conditions. Accordingly, interpretation emphasises physiological coherence and consistency of predictors across analytical stages rather than marginal differences between individual top-ranked model configurations. Relative model rankings and dominant indicator families remained qualitatively consistent across repeated cross-validation runs, indicating that observed recurrence patterns are not driven by a single data partition.

Table 6. Top 10 constrained multivariate yield models for wheat, ranked by coefficient of determination (R^2). Corresponding root mean square error (RMSE) values are expressed in kg stremma^{-1}.

k	Predictors	Model	R^2	RMSE
4	NDWI2+NIR_DIFF+NDI451+BNDVI1	OLS	0.824	52.80
3	NDWI2+NIR_DIFF+PSSRA2	OLS	0.818	53.72
3	Ddays+NDWI2+RE3_DIFF	OLS	0.816	53.99
3	GNDVI_RATE+NDWI2+RED_DIFF	OLS	0.813	54.35
3	NDWI2+NIR_DIFF+NDI451	OLS	0.813	54.39
3	NDWI2+NIR_DIFF+PSSRA2	Huber	0.813	54.43
3	NDWI2+NIR_DIFF+PSSRA2	ARD	0.809	54.96
3	NDWI2+NIR_DIFF+NDI451	ARD	0.805	55.52
3	Ddays+NDWI2+RE3_DIFF	Huber	0.804	55.70
4	Ddays+NDWI2+NIR_DIFF+NVDI_RATIO	ExtraTrees	0.803	55.77

Table 7. Top 10 constrained multivariate yield models for cotton, ranked by coefficient of determination (R^2). Corresponding root mean square error (RMSE) values are expressed in kg stremma^{-1}.

k	Predictors	Model	R^2	RMSE
3	GDD1+NDVI2_SQ+RED1	ExtraTrees	0.758	29.79
2	GDD_DIFF+NDVI_MEAN	ExtraTrees	0.758	29.79
3	GDD_DIFF+NDVI_MEAN+MCARI2xNDRE2	ExtraTrees	0.753	30.13
3	GDD1+NDVI2_SQ+MCARI2xNDRE2	ExtraTrees	0.751	30.23
3	GDD1+NDVI2_SQ+GNDVI1	ExtraTrees	0.748	30.45
4	GDD1+NDVI2_SQ+RE31+MCARI2xNDRE2	ExtraTrees	0.745	30.61
4	Ddays+GDD_DIFF+NDVI1+NDWI2	ExtraTrees	0.744	30.64
2	GDD2+NDVI_MEAN	ExtraTrees	0.744	30.67
4	GDD1+NDVI2+GNDVI1+RE3_DIFF	ExtraTrees	0.740	30.90
3	GDD_DIFF+NDI452+MSAVI1	ExtraTrees	0.738	30.99

3.4. Variable Recurrence Across Constrained Multivariate Models

Table 8 summarises the frequency with which individual variables appear across the top 100 constrained multivariate models for wheat and cotton. Frequencies are reported separately for each crop and represent the number of occurrences of each variable across the selected model set. Recurrence frequency is reported as a descriptive indicator of stability within the constrained model space and does not imply statistical importance, causal dominance, or independent explanatory power.

 doi:10.20944/preprints202604.0463.v1

Table 8. Frequency of variable occurrence in the top 100 constrained multivariate models.

Wheat		Cotton	
Variable	Occurrences (n)	Variable	Occurrences (n)
NDWI2	67	GDD_DIFF	45
RE3_DIFF	50	GDD1	31
NIR_DIFF	36	GDD2	21
NDWI_MEAN	20	NDVI_MEAN	15
PSSRA2	16	NDI452	13
GDD1	12	NDVI2_SQ	13
NDWI_RATE	12	NDVI2	12
Ddays	11	NDWI2	12
NDI451	10	MCARI2xNDRE2	11
BNDVI1	9	NDVIxNDWI	11
RE3_1	9	NDVI1	9
GNDVI_RATE	6	IRECI2	7
NDWI_DIFF	6	RED1	7
NDVI_RATIO	6	BNDVI1	6
NDVI_RATE	5	GNDVI1	6
GDD_DIFF	4	NDWI_MEAN	6
GDD2	4	RE3_DIFF	6
NIR2	4	RE31	6
PSSRA1	4	RED2	6
RE3_2	4	MSAVI1	5
MCARI1	3	NIR1	5
MCARI2	3	BNDVI2	4
RED1	3	Ddays	4
NDVIxNDWI	2	GNDVI2	4
NIR1	2	MCARI1	4
GNDVI1	1	MCARI2	4
IRECI2	1	NDI451	4
MSAVI2	1	NDVI_RATE	4
NDVI_MEAN	1	PSSRA1	4
NDVI1	1	IRECI1	3
RED_DIFF	1	NDWI1	3
		NIR_DIFF	3
		PSSRA2	3
		GNDVI_RATE	2
		NDVI_DIFF	2
		NDWI_DIFF	2
		NDVI_RATIO	2
		GNDVI_DIFF	1
		MSAVI2	1
		NIR2	1
		RE32	1
		RED_DIFF	1

For wheat, the highest recurrence is observed for NDWI2, which appears in 67 of the top 100 models, followed by RE3_DIFF (50 occurrences) and NIR_DIFF (36 occurrences). Additional variables with notable recurrence include NDWI_MEAN, PSSRA2, NDWI_RATE, GDD1, and Ddays, each appearing in more than ten models. A broader set of variables appears less frequently, with multiple predictors occurring fewer than five times across the model set. For cotton, the most frequently occurring variable across the top 100 models is GDD_DIFF, with 45 occurrences, followed by GDD1

 doi:10.20944/preprints202604.0463.v1

(31 occurrences) and GDD2 (21 occurrences). Several vegetation indices and interaction terms, including NDVI_MEAN, NDVI2_SQ, NDI452, NDVI2, NDWI2, MCARI2xNDRE2, and NDVIxNDWI, also appear repeatedly across the model set, with occurrence counts ranging from 11 to 15. Additional variables appear sporadically, with lower frequencies distributed across a wide range of spectral, phenological, and derived predictors.

Across both crops, Table 8 and Figure 5 report the full distribution of variable recurrence within the constrained multivariate model space. No ranking or weighting beyond raw frequency is applied, and all counts reflect model inclusion only.

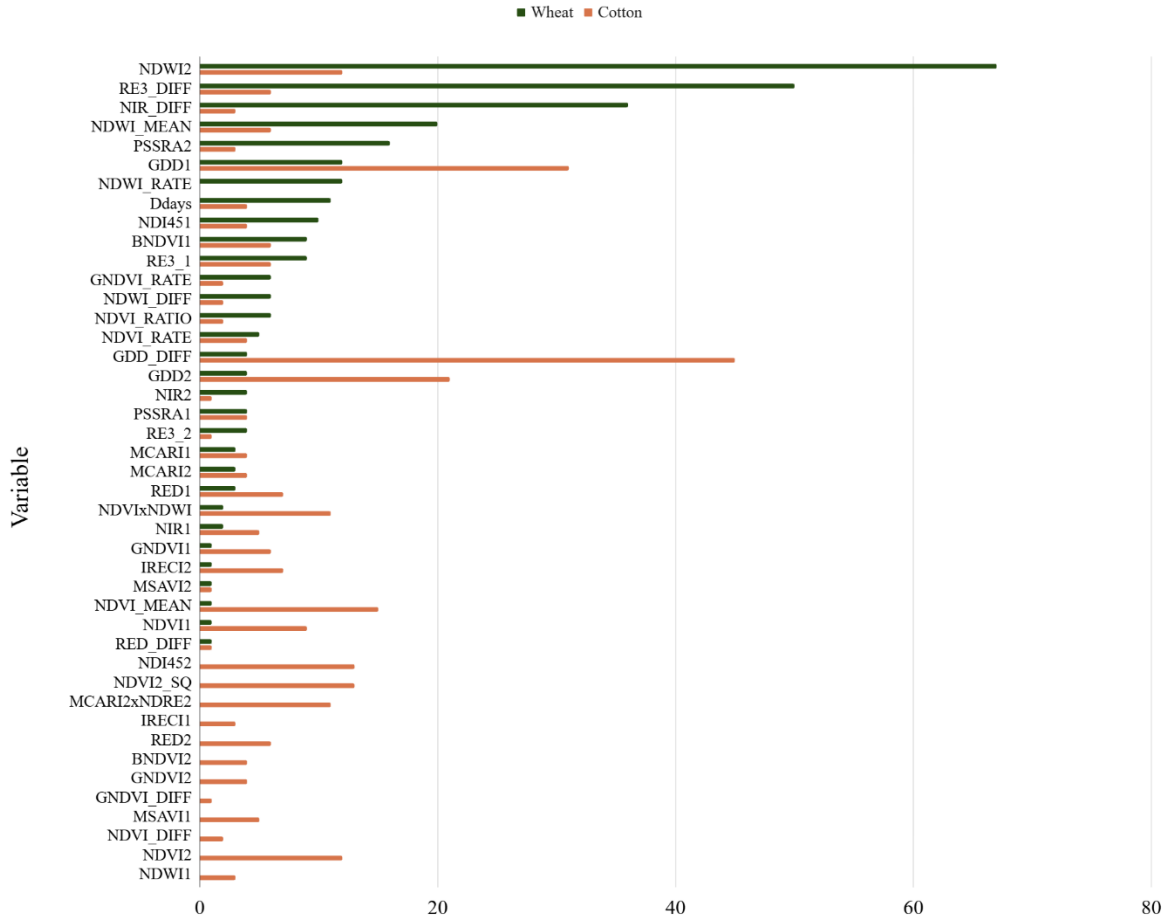

Figure 5. Wheat vs. cotton variable occurrence. Frequency of spectral, thermal, and temporal variables in the modeling workflow for wheat (green) and cotton (orange), illustrating differences in dominant predictors between the two crops.

4. Discussion

4.1. Crop-Specific Yield Drivers Under a Harmonised Sentinel-2 Indicator Framework

Under a fully harmonised Sentinel-2 indicator framework, yield–spectral relationships exhibit clearly distinct, crop-specific patterns, even when observational and analytical conditions are held constant [16]. Crop yield integrates multiple physiological processes whose relative importance varies across crop types, phenological cycles, and environmental conditions, a pattern consistently reported in both agronomic and satellite-based yield studies [44]. By analysing two contrasting crops under identical observational and analytical conditions within a unified indicator framework, this study isolates crop-specific physiological drivers of yield variability with minimal methodological interference, which is often a limiting factor in multi-crop yield estimation studies due to differences in acquisition timing, feature selection, and modeling strategy [45,46]. Within this controlled

 doi:10.20944/preprints202604.0463.v1

framework, wheat yield variability was most strongly associated with water-sensitive and canopy-structure-related indicators, whereas cotton yield variability was dominated by thermal accumulation metrics.

These findings are consistent with a broad body of literature describing wheat yield formation as highly sensitive to seasonal water availability, canopy development, and moisture stress during critical growth stages, particularly under Mediterranean and semi-arid conditions [31,47,48]. The prominence of NDWI-derived variables and soil- and canopy-adjusted greenness indices reflects the direct roles of vegetation water status and canopy structure in regulating biomass accumulation and grain filling. NDWI is explicitly designed to capture variations in vegetation water content and canopy moisture [36], and its relevance for diagnosing crop water stress and productivity limitations has been demonstrated in both field-based and satellite-driven studies [49]. The repeated appearance of red-edge and near-infrared change metrics further aligns with studies demonstrating that these spectral regions are particularly sensitive to chlorophyll dynamics and canopy structural variation closely linked to yield formation in cereals [6,43].

In contrast, cotton yield variability was primarily associated with thermal accumulation indicators, consistent with agronomic evidence that cotton development, flowering, and boll retention are strongly regulated by cumulative heat exposure and temperature-driven phenological progression [50–53]. The dominance of growing degree day (GDD) variables across analytical stages supports findings from both field-based and remote sensing studies that identify thermal time as a primary control on cotton yield potential and yield losses under heat-stress conditions [52,54]. The co-occurrence of selected spectral indicators, including NDVI- and pigment-sensitive metrics, suggests that canopy condition provides complementary explanatory information once phenological timing and thermal exposure are accounted for, as reported in recent cotton monitoring and yield estimation studies using optical remote sensing [32,54,55]. This contrasts with wheat highlights the shift from water-limited to temperature-driven yield control mechanisms across seasonal cropping systems.

Overall, these results demonstrate that, when methodological variability is minimised, crop physiology emerges as the primary driver of yield–spectral relationships. This finding reinforces the importance of selecting crop-specific indicators and supports the use of physiologically grounded, interpretable feature sets in remote sensing applications for precision agriculture.

4.2. Consistency of Indicator Behavior Across Analytical Stages

Throughout the following analysis, individual model rankings are not interpreted deterministically. Given the small sample size and the presence of correlated predictors, multiple near-equivalent model configurations are expected. Consequently, interpretation focuses on recurrent indicator families and their physiological relevance across analytical stages rather than on any single ‘best-performing’ model.

A central contribution of this study is the explicit examination of indicator behavior across multiple analytical stages, including correlation analysis, univariate regression, constrained multivariate modeling, and frequency-based recurrence within the top model set. Many yield-estimation studies prioritize reporting a single optimized model, often focusing on predictive accuracy, while providing limited insight into whether identified predictors represent stable yield drivers or artifacts of a particular modeling configuration [28,46]. Such approaches can obscure the agronomic relevance of individual indicators, particularly when complex or high-dimensional models are applied to relatively small datasets. By contrast, the present results demonstrate that certain indicator families remain consistently dominant across analytical stages, while others exhibit stage-specific or context-dependent relevance.

For wheat, NDWI-based indicators consistently rank among the strongest predictors in correlation, univariate, and multivariate analyses and exhibit high recurrence within the constrained model space. This multi-stage consistency supports the interpretation that vegetation water status constitutes a robust and physiologically meaningful yield driver under the study conditions, in

 doi:10.20944/preprints202604.0463.v1

agreement with studies emphasising the role of soil moisture availability and evaporative demand in regulating cereal productivity, biomass accumulation, and grain filling [31,56]. For cotton, the repeated recurrence of GDD-based predictors across analytical stages reinforces agronomic evidence that temperature-driven development and cumulative heat exposure exert persistent control over yield outcomes across seasons [47,50,54]. The persistence of these indicator families across analytical stages strengthens confidence that they represent stable yield drivers rather than model-dependent effects.

Despite variability in field parcels and growing seasons, several indicators were consistently observed across models, suggesting that remote sensing signals can capture stable patterns in crop performance under heterogeneous field conditions. This consistency further supports the robustness of the identified indicator families and highlights their potential relevance for operational applications in precision agriculture, where variability in field conditions is inherent.

4.3. Reconciling Correlation Strength with Multivariate Recurrence

An important finding of this study is that variables exhibiting the strongest correlation with yield are not always those that dominate recurrence within the constrained multivariate model space. While correlation-based screening remains a widely used initial step in yield modeling, it primarily captures linear or monotonic associations and may not fully reflect the contribution of predictors within multivariate, physiologically structured relationships. Recent work in remote sensing–based yield modeling and explainable feature analysis has highlighted that correlation-based rankings can overlook variables whose explanatory contribution emerges primarily through complementary or conditional effects when combined with other predictors [57,58]. As a result, reliance on correlation strength alone may underestimate the agronomic relevance of indicators that contribute to yield variability through interaction with distinct physiological processes. Strong correlation does not necessarily imply the maximum explanatory contribution in multivariate settings, particularly when key drivers, such as thermal accumulation and water status, capture distinct, partially orthogonal dimensions of crop response.

In wheat, although NDWI_MEAN and NDWI1 exhibit strong correlation with yield, recurrence analysis highlights NDWI2, RE3_DIFF, and NIR_DIFF as more frequent components of multivariate model configurations. This pattern suggests that phenologically targeted indicators, particularly those capturing later-stage canopy water status and inter-date canopy dynamics, provide greater explanatory value when combined with complementary predictors than static or season-averaged metrics alone. Similar findings have been reported in studies emphasising the importance of growth-stage-specific indicators and intra-seasonal canopy dynamics for yield explanation, particularly under water-limited conditions where the timing of stress, rather than its seasonal average, governs yield outcomes [3,30].

In cotton, thermal variables remain dominant across both correlation ranking and recurrence analysis, indicating that thermal accumulation provides a strong and largely non-substitutable explanatory signal under the examined conditions. This persistence suggests that temperature-driven phenological progression is a primary constraint on yield variability, while spectral indicators provide secondary, complementary information on canopy condition within this thermal framework. Recent cotton-focused studies similarly report that cumulative heat exposure governs key developmental processes, while spectral indicators primarily capture responses conditioned by temperature-driven growth dynamics [54].

Overall, these results highlight that multivariate recurrence provides a complementary perspective to correlation-based analysis, enabling the identification of physiologically meaningful predictors that may not be apparent from correlation strength alone. This reinforces the importance of moving beyond single-metric ranking approaches toward integrated, multi-stage evaluation frameworks when interpreting yield–spectral relationships.

 doi:10.20944/preprints202604.0463.v1

4.4. Implications for Indicator Selection and Agronomic Interpretability

The results reinforce the broader argument that yield estimation from remote sensing is not solely a modeling problem, but fundamentally an indicator interpretation and physiological attribution problem. A recurring limitation in recent yield-modeling literature is the emphasis on maximising predictive accuracy through large, high-dimensional feature sets and complex model architectures, often with limited physiological justification and reduced transparency [20,28,52,57]. While such approaches can achieve high predictive performance, they are frequently difficult to translate into actionable agronomic insight, particularly in precision agriculture contexts where decision relevance, trust, and operational interpretability are critical [23,28,57].

The present findings support a more parsimonious and physiologically grounded strategy for indicator selection. Across both crops, a limited set of carefully selected indicators explained a substantial proportion of yield variability, demonstrating that simple, interpretable models may be sufficient for field-level crop monitoring. This result highlights that model complexity is not a prerequisite for achieving meaningful explanatory performance, particularly when predictors align with key physiological processes, such as vegetation water status and thermal accumulation.

For wheat, prioritising indicators related to vegetation water status and canopy structural dynamics aligns with operational monitoring practices focused on drought stress detection, canopy development, and biomass accumulation, which are increasingly adopted in satellite-based decision-support systems for cereal production [3,11,31]. For cotton, combining thermal accumulation metrics with complementary canopy spectral indicators reflects established and modern agronomic approaches that integrate phenological tracking with canopy condition to contextualise yield outcomes and management decisions [54].

Importantly, the use of constrained multivariate combinations demonstrates that improved yield explanation can be achieved without resorting to high-dimensional or opaque modeling approaches. This finding supports the development of transparent, robust, and crop-aware modeling strategies that are better aligned with the practical requirements of precision agriculture. In operational contexts, where data availability, computational resources, and user interpretability are often limiting factors, such parsimonious approaches provide a more scalable and transferable alternative to complex modeling frameworks [20,57].

4.5. Value of Controlled Cross-Crop Comparison Under Identical Data Structure

Cross-crop comparisons in yield modeling are often difficult to interpret because existing studies frequently differ in acquisition timing, predictor definitions, spatial aggregation, and modelling strategies across crops, making it challenging to disentangle crop physiology from methodological effects [15,31,46,59]. As a result, reported differences in yield–spectral relationships across crops are often confounded by variations in analytical design rather than reflecting genuine biological contrasts.

By holding the feature space, data structure, and analytical workflow constant, this study provides empirical evidence that differences in dominant yield drivers are primarily attributable to crop physiology and seasonal context rather than to methodological variability. This controlled comparison strengthens the interpretability of crop-specific findings and highlights the importance of analysing yield–spectral relationships under consistent methodological assumptions. Similar needs for harmonised, crop-comparable analytical frameworks have been emphasised in recent multi-crop and large-scale yield monitoring studies, particularly in the context of operational remote sensing applications [57,60].

As such, the framework presented here offers a transferable template for comparative yield analysis across crops, enabling future studies to more effectively disentangle biological signal from analytical design and to assess the generality or crop-specificity of spectral yield drivers under controlled observational conditions [3,15].

 doi:10.20944/preprints202604.0463.v1

4.6. Limitations and Future Research

Several limitations should be considered when interpreting the results of this study. First, the number of field–year observations is relatively limited, which constrains the complexity of multivariate models and restricts the exploration of higher-order interactions. Although repeated cross-validation was applied to support robust model evaluation, the identified indicator rankings and recurrence patterns remain conditioned by the available sample size and site-specific context. This limitation is common in field-scale and experimental yield studies based on satellite observations, where data availability is often constrained by monitoring logistics and experimental design [20,46].

Second, the analysis relies on two Sentinel-2 acquisitions per growing season. While this design supports interpretability and phenological targeting, it may not capture short-term stress events, transient water deficits, or rapid canopy changes that influence yield formation, particularly under variable weather conditions [3]. Future work could evaluate whether higher-temporal-resolution time series metrics, such as seasonal integrals, peak timing, or curve-shape descriptors derived from dense satellite observations, improve indicator stability and explanatory power without compromising interpretability [30].

Third, the modeling framework focuses exclusively on spectral and phenological indicators, without explicitly incorporating soil properties, management practices, or detailed weather variability beyond thermal accumulation. While this design was intentional to isolate the contribution of remote sensing–derived indicators under controlled conditions, it limits the ability to disentangle environmental- and management-driven effects on yield variability. Integrating spectral data with soil, climate, and management variables represents a key direction for future work and may enhance both explanatory robustness and operational relevance in precision agriculture applications [15,20].

Finally, the cross-validation strategy was applied at the field–year level without explicitly accounting for temporal or spatial dependence. As a result, observations from different years within the same field may appear in both the training and testing folds, potentially leading to optimistic performance estimates. Future studies could implement stricter validation schemes, such as leave-one-year-out or field-blocked cross-validation, to further assess the generalisation capacity of the identified indicator relationships under more independent conditions.

Despite these limitations, the study provides a controlled and interpretable framework for analysing yield–spectral relationships, enabling the identification of stable, physiologically meaningful indicator families across crops. Future research building on this approach can extend its applicability by incorporating additional data sources, increasing temporal resolution, and evaluating robustness across broader agroecological contexts.

5. Conclusions

Under a fully harmonised Sentinel-2 indicator framework applied consistently across wheat and cotton, this study demonstrates that yield–spectral relationships are strongly crop-dependent when examined under identical observational and analytical conditions. By controlling for methodological variability, the analysis isolates crop physiology as the primary driver of differences in indicator performance.

Wheat yield variability was most consistently associated with water-sensitive and canopy-related indicators, reflecting the importance of vegetation water status and structural development during critical growth stages. In contrast, cotton yield variability was dominated by thermal accumulation metrics, highlighting the central role of temperature-driven phenological progression in warm-season crop yield formation. These contrasting indicator patterns can be explained by fundamental differences in crop physiology, phenology, and water demand between winter cereals and summer crops. Wheat, cultivated as a winter cereal under Mediterranean conditions, develops during cooler, wetter periods, when water availability and canopy dynamics play a dominant role,

 doi:10.20944/preprints202604.0463.v1

whereas cotton develops under warmer conditions, where cumulative heat exposure becomes the primary limiting factor.

Importantly, these crop-specific indicator families remained stable across multiple analytical stages, including correlation analysis, univariate regression, and constrained multivariate modeling. Their repeated occurrence across top-performing model configurations indicates that they are robust and physiologically meaningful yield drivers rather than artifacts of a particular modeling approach. Despite variability in field parcels and growing seasons, a limited set of indicators consistently explained a substantial proportion of yield variability, demonstrating that parsimonious and interpretable models can effectively support field-level crop monitoring.

More broadly, the results highlight that yield estimation from remote sensing is not solely a modeling challenge, but fundamentally an issue of indicator selection and physiological interpretation. The findings support the use of crop-aware, physiologically grounded indicator frameworks and demonstrate that simple, well-targeted predictor sets can provide substantial explanatory power without reliance on complex or opaque modeling approaches.

The harmonized analytical framework presented in this study offers a transferable approach for comparative yield analysis across crops, enabling clearer separation of biological signal from methodological artifacts. This is particularly relevant for operational precision agriculture applications, where robust, interpretable, and scalable methods are required to support multi-crop monitoring under heterogeneous field conditions.

Author Contributions: Conceptualization, E.P. and A.O.; methodology, E.P. and A.O.; software, E.P., A.O. and M.A.; validation, A.O. and M.A.; formal analysis, E.P., A.O. and A.K.; data curation, E.P.; writing—original draft preparation, A.O., E.P., M.A. and A.K.; writing—review and editing, E.P., A.O. and M.A.; visualization, E.P., A.K.; supervision, E.P.; project administration, E.P. All authors have read and agreed to the published version of the manuscript.

Funding: This study is part of the AgroSense Project (16476), carried out within the framework of the National Recovery and Resilience Plan Greece 2.0, funded by the European Union - NextGenerationEU (Implementation body: HFRI).

Data Availability Statement: Data will be made available on request.

Acknowledgments: The authors acknowledge the Copernicus Programme for providing access to Earth-observation data, as well as the Corine Land Cover 2018 dataset obtained through the Copernicus Land Monitoring Service.

Conflicts of Interest: The authors declare no conflicts of interest.

Abbreviations

The following abbreviations are used in this manuscript:

ARD	Automatic Relevance Determination
BNDVI	Blue Normalized Difference Vegetation Index
Ddays	Days between Sentinel-2 image acquisitions
ESA	European Space Agency
EMY	Hellenic National Meteorological Service
GDD	Growing Degree Days
GNDVI	Green Normalized Difference Vegetation Index
IRECI	Inverted Red-Edge Chlorophyll Index
MCARI	Modified Chlorophyll Absorption Ratio Index

 doi:10.20944/preprints202604.0463.v1

MSAVI	Modified Soil-Adjusted Vegetation Index
NDI45	Normalized Difference Index
NDRE	Normalized Difference Red-Edge Index
NDVI	Normalized Difference Vegetation Index
NDWI	Normalized Difference Water Index
OLS	Ordinary Least Squares
PSSRA	Pigment-Specific Simple Ratio (chlorophyll a)
RE	Red-edge spectral band
RMSE	Root Mean Square Error
R^2	Coefficient of determination
S2	Sentinel-2
SWIR	Short-Wave Infrared

References

1. Lobell, D.B.; Azzari, G.; Burke, M.; Gourlay, S.; Jin, Z.; Kilic, T.; Murray, S. Eyes in the Sky, Boots on the Ground: Assessing Satellite- and Ground-Based Approaches to Crop Yield Measurement and Analysis. *American Journal of Agricultural Economics* **2020**, *102*, 202–219, doi:10.1093/ajae/aaz051.
2. Psomiadis, E.; Toubaridis, C.; Avramidou, M. Combining Multispectral Data from Unmanned Aerial System and Sentinel-2 for Kiwifruit and Cotton Monitoring and Yield Assessment. In Proceedings of the IGARSS 2024 - 2024 IEEE International Geoscience and Remote Sensing Symposium; July 2024; pp. 4312–4315.
3. Wu, B.; Zhang, M.; Zeng, H.; Tian, F.; Potgieter, A.B.; Qin, X.; Yan, N.; Chang, S.; Zhao, Y.; Dong, Q.; et al. Challenges and Opportunities in Remote Sensing-Based Crop Monitoring: A Review. *National Science Review* **2023**, *10*, nwac290, doi:10.1093/nsr/nwac290.
4. Psomiadis, E.; Avramidou, M.; Kavvadias, A.; Oikonomou, A. Pairing Multiple Remote Sensors for Crop Management and Agricultural Sustainability. In Proceedings of the Remote Sensing for Agriculture, Ecosystems, and Hydrology XXVII; SPIE, October 30 2025; Vol. 13666, pp. 89–98.
5. Velazquez-Chavez, L.J.; Daccache, A.; Mohamed, A.Z.; Centritto, M. Plant-Based and Remote Sensing for Water Status Monitoring of Orchard Crops: Systematic Review and Meta-Analysis. *Agricultural Water Management* **2024**, *303*, 109051, doi:10.1016/j.agwat.2024.109051.
6. Clevers, J.G.P.W.; Gitelson, A. Remote Estimation of Crop and Grass Chlorophyll and Nitrogen Content Using Red-Edge Bands on Sentinel-2 and -3. *International Journal of Applied Earth Observation and Geoinformation* **2013**, *23*, 344–351, doi:10.1016/j.jag.2012.10.008.
7. Darra, N.; Espejo-Garcia, B.; Psiroukis, V.; Psomiadis, E.; Fountas, S. Spectral Bands vs. Vegetation Indices: An AutoML Approach for Processing Tomato Yield Predictions Based on Sentinel-2 Imagery. *Smart Agricultural Technology* **2025**, *10*, 100805, doi:10.1016/j.atech.2025.100805.
8. Ronchetti, G.; Manfron, G.; Weissteiner, C.J.; Seguini, L.; Nisini Scacchiafichi, L.; Panarello, L.; Baruth, B. Remote Sensing Crop Group-Specific Indicators to Support Regional Yield Forecasting in Europe. *Computers and Electronics in Agriculture* **2023**, *205*, 107633, doi:10.1016/j.compag.2023.107633.
9. Alexandris, S.; Psomiadis, E.; Proutsos, N.; Philippopoulos, P.; Charalampopoulos, I.; Kakaletris, G.; Papoutsi, E.-M.; Vassilakis, S.; Paraskevopoulos, A. Integrating Drone Technology into an Innovative Agrometeorological Methodology for the Precise and Real-Time Estimation of Crop Water Requirements. *Hydrology* **2021**, *8*, doi:10.3390/hydrology8030131.
10. Iordanoglou, K.; Alexopoulou, E.; Psomiadis, E. Using Multisource and Multiscale Remote Sensing Data for Miscanthus and Switchgrass Yield and Biomass Production Estimation. In Proceedings of the Remote Sensing for Agriculture, Ecosystems, and Hydrology XXVII; SPIE, October 30 2025; Vol. 13666, pp. 264–274.
11. Hatfield, J.L.; Prueger, J.H. Temperature Extremes: Effect on Plant Growth and Development. *Weather and Climate Extremes* **2015**, *10*, 4–10, doi:10.1016/j.wace.2015.08.001.
12. Sinclair, T.; Rufty, T. Nitrogen and Water Resources Commonly Limit Crop Yield Increases, Not Necessarily Plant Genetics. *Global Food Security* **2012**, *1*, 94–98, doi:10.1016/j.gfs.2012.07.001.
13. Cossani, C.; Sadras, V. Water–Nitrogen Colimitation in Grain Crops. *Advances in Agronomy* **2018**, *150*, 231, doi:10.1016/bs.agron.2018.02.004.

 doi:10.20944/preprints202604.0463.v1

14. Colonna, R.; Genzano, N.; Ciancia, E.; Filizzola, C.; Fiorentino, C.; D'Antonio, P.; Tramutoli, V. A Method to Determine the Optimal Period for Field-Scale Yield Prediction Using Sentinel-2 Vegetation Indices. *Land* **2024**, *13*, 1818, doi:10.3390/land13111818.
15. Peng, B.; Guan, K.; Zhou, W.; Jiang, C.; Frankenberg, C.; Sun, Y.; He, L.; Köhler, P. Assessing the Benefit of Satellite-Based Solar-Induced Chlorophyll Fluorescence in Crop Yield Prediction. *International Journal of Applied Earth Observation and Geoinformation* **2020**, *90*, 102126, doi:10.1016/j.jag.2020.102126.
16. Ronchetti, G.; Manfron, G.; Weissteiner, C.J.; Seguini, L.; Nisini Scacchiafichi, L.; Panarello, L.; Baruth, B. Remote Sensing Crop Group-Specific Indicators to Support Regional Yield Forecasting in Europe. *Computers and Electronics in Agriculture* **2023**, *205*, 107633, doi:10.1016/j.compag.2023.107633.
17. Mokhtari, A.; Yang, H.; Croft, H.; Luca, S.V.; Li, F.; Minceva, M.; Schmidthalter, U.; Yu, K. Satellite-Based Winter Wheat Yield Estimation with a Newly Parameterized LUE Model Based on Crop Water Status and Leaf Chlorophyll Content. *Field Crops Research* **2025**, *333*, 110106, doi:10.1016/j.fcr.2025.110106.
18. Psomiadis, E.; Papazoglou, G.E.; Alexopoulou, E. Integrating Earth Observation for the Precise Monitoring of Novel Farming Systems and Water Harvesting Techniques to Address Extreme Drought in the Mediterranean Region, Including Saline and Drought-Resilient Species: WaterMellon Project. In Proceedings of the Earth Resources and Environmental Remote Sensing/GIS Applications XVI; SPIE, October 28 2025; Vol. 13671, pp. 528–531.
19. Ryo, M. Explainable Artificial Intelligence and Interpretable Machine Learning for Agricultural Data Analysis. *Artificial Intelligence in Agriculture* **2022**, *6*, 257–265, doi:10.1016/j.aiia.2022.11.003.
20. Benos, L.; Tagarakis, A.C.; Dolias, G.; Berruto, R.; Kateris, D.; Bochtis, D. Machine Learning in Agriculture: A Comprehensive Updated Review. *Sensors* **2021**, *21*, 3758, doi:10.3390/s21113758.
21. Liakos, K.G.; Busato, P.; Moshou, D.; Pearson, S.; Bochtis, D.; Liakos, K.G.; Busato, P.; Moshou, D.; Pearson, S.; Bochtis, D. Machine Learning in Agriculture: A Review. *Sensors* **2018**, *18*, doi:10.3390/s18082674.
22. van Klompenburg, T.; Kassahun, A.; Catal, C. Crop Yield Prediction Using Machine Learning: A Systematic Literature Review. *Computers and Electronics in Agriculture* **2020**, *177*, 105709, doi:10.1016/j.compag.2020.105709.
23. Ryo, M. Explainable Artificial Intelligence and Interpretable Machine Learning for Agricultural Data Analysis. *Artificial Intelligence in Agriculture* **2022**, *6*, 257–265, doi:10.1016/j.aiia.2022.11.003.
24. Hu, T.; Zhang, X.; Bohrer, G.; Liu, Y.; Zhou, Y.; Martin, J.; Li, Y.; Zhao, K. Crop Yield Prediction via Explainable AI and Interpretable Machine Learning: Dangers of Black Box Models for Evaluating Climate Change Impacts on Crop Yield. *Agricultural and Forest Meteorology* **2023**, *336*, 109458, doi:10.1016/j.agrformet.2023.109458.
25. van Klompenburg, T.; Kassahun, A.; Catal, C. Crop Yield Prediction Using Machine Learning: A Systematic Literature Review. *Computers and Electronics in Agriculture* **2020**, *177*, 105709, doi:10.1016/j.compag.2020.105709.
26. Benos, L.; Tagarakis, A.C.; Dolias, G.; Berruto, R.; Kateris, D.; Bochtis, D. Machine Learning in Agriculture: A Comprehensive Updated Review. *Sensors* **2021**, *21*, 3758, doi:10.3390/s21113758.
27. Hu, T.; Zhang, X.; Bohrer, G.; Liu, Y.; Zhou, Y.; Martin, J.; Li, Y.; Zhao, K. Crop Yield Prediction via Explainable AI and Interpretable Machine Learning: Dangers of Black Box Models for Evaluating Climate Change Impacts on Crop Yield. *Agricultural and Forest Meteorology* **2023**, *336*, 109458, doi:10.1016/j.agrformet.2023.109458.
28. Atzberger, C. Advances in Remote Sensing of Agriculture: Context Description, Existing Operational Monitoring Systems and Major Information Needs. *Remote Sensing* **2013**, *5*, 949–981, doi:10.3390/rs5020949.
29. Jeong, J.H.; Resop, J.P.; Mueller, N.D.; Fleisher, D.H.; Yun, K.; Butler, E.E.; Timlin, D.J.; Shim, K.-M.; Gerber, J.S.; Reddy, V.R.; et al. Random Forests for Global and Regional Crop Yield Predictions. *PLOS ONE* **2016**, *11*, e0156571, doi:10.1371/journal.pone.0156571.
30. Cai, Y.; Guan, K.; Peng, J.; Wang, S.; Seifert, C.; Wardlow, B.; Li, Z. A High-Performance and in-Season Classification System of Field-Level Crop Types Using Time-Series Landsat Data and a Machine Learning Approach. *Remote Sensing of Environment* **2018**, *210*, 35–47, doi:10.1016/j.rse.2018.02.045.

 doi:10.20944/preprints202604.0463.v1

31. Ceglar, A.; Toreti, A.; Lecerf, R.; Van der Velde, M.; Dentener, F. Impact of Meteorological Drivers on Regional Inter-Annual Crop Yield Variability in France. *Agricultural and Forest Meteorology* **2016**, *216*, 58–67, doi:10.1016/j.agrformet.2015.10.004.
32. Vaz, C.M.P.; Ferreira, E.J.; Speranza, E.A.; Franchini, J.C.; Naime, J. de M.; Inamasu, R.Y.; Lopes, I. de O.N.; das Chagas, S.; Schelp, M.X.; Vecchi, L.; et al. Cotton Yield Map Prediction Using Sentinel-2 Satellite Imagery in the Brazilian Cerrado Production System. *AgriEngineering* **2025**, *7*, 390, doi:10.3390/agriengineering7110390.
33. McMaster, G.S.; Wilhelm, W.W. Growing Degree-Days: One Equation, Two Interpretations. *Agricultural and Forest Meteorology* **1997**, *87*, 291–300, doi:10.1016/S0168-1923(97)00027-0.
34. Rouse, J.W.; Haas, R.H.; Schell, J.A.; Deering, D.W. Monitoring Vegetation Systems in the Great Plains with ERTS.; January 1 1974.
35. Gitelson, A.A.; Kaufman, Y.J.; Merzlyak, M.N. Use of a Green Channel in Remote Sensing of Global Vegetation from EOS-MODIS. *Remote Sensing of Environment* **1996**, *58*, 289–298, doi:10.1016/S0034-4257(96)00072-7.
36. Gao, B. NDWI—A Normalized Difference Water Index for Remote Sensing of Vegetation Liquid Water from Space. *Remote Sensing of Environment* **1996**, *58*, 257–266, doi:10.1016/S0034-4257(96)00067-3.
37. Barnes, E.; Colaizzi, P.; Haberland, J.; Waller, P. Coincident Detection of Crop Water Stress, Nitrogen Status, and Canopy Density Using Ground Based Multispectral Data. **2000**.
38. Frampton, W.J.; Dash, J.; Watmough, G.; Milton, E.J. Evaluating the Capabilities of Sentinel-2 for Quantitative Estimation of Biophysical Variables in Vegetation. *ISPRS Journal of Photogrammetry and Remote Sensing* **2013**, *82*, 83–92, doi:10.1016/j.isprsjprs.2013.04.007.
39. Daughtry, C.S.T.; Walthall, C.L.; Kim, M.S.; de Colstoun, E.B.; McMurtrey, J.E. Estimating Corn Leaf Chlorophyll Concentration from Leaf and Canopy Reflectance. *Remote Sensing of Environment* **2000**, *74*, 229–239, doi:10.1016/S0034-4257(00)00113-9.
40. Blackburn, G.A. Quantifying Chlorophylls and Caroteniods at Leaf and Canopy Scales: An Evaluation of Some Hyperspectral Approaches. *Remote Sensing of Environment* **1998**, *66*, 273–285, doi:10.1016/S0034-4257(98)00059-5.
41. Qi, J.; Chehbouni, A.; Huete, A.R.; Kerr, Y.H.; Sorooshian, S. A Modified Soil Adjusted Vegetation Index. *Remote Sensing of Environment* **1994**, *48*, 119–126, doi:10.1016/0034-4257(94)90134-1.
42. Tucker, C.J. Red and Photographic Infrared Linear Combinations for Monitoring Vegetation. *Remote Sensing of Environment* **1979**, *8*, 127–150, doi:10.1016/0034-4257(79)90013-0.
43. Delegido, J.; Verrelst, J.; Alonso, L.; Moreno, J. Evaluation of Sentinel-2 Red-Edge Bands for Empirical Estimation of Green LAI and Chlorophyll Content. *Sensors* **2011**, *11*, 7063–7081, doi:10.3390/s110707063.
44. Lobell, D.B.; Schlenker, W.; Costa-Roberts, J. Climate Trends and Global Crop Production Since 1980. *Science* **2011**, *333*, 616–620, doi:10.1126/science.1204531.
45. Lobell, D.B. The Use of Satellite Data for Crop Yield Gap Analysis. *Field Crops Research* **2013**, *143*, 56–64, doi:10.1016/j.fcr.2012.08.008.
46. Lobell, D.B.; Thau, D.; Seifert, C.; Engle, E.; Little, B. A Scalable Satellite-Based Crop Yield Mapper. *Remote Sensing of Environment* **2015**, *164*, 324–333, doi:10.1016/J.RSE.2015.04.021.
47. Asseng, S.; Ewert, F.; Martre, P.; Rötter, R.P.; Lobell, D.B.; Cammarano, D.; Kimball, B.A.; Ottman, M.J.; Wall, G.W.; White, J.W.; et al. Rising Temperatures Reduce Global Wheat Production. *Nature Clim Change* **2015**, *5*, 143–147, doi:10.1038/nclimate2470.
48. Mokhtari, A.; Yang, H.; Croft, H.; Luca, S.V.; Li, F.; Minceva, M.; Schmidthalter, U.; Yu, K. Satellite-Based Winter Wheat Yield Estimation with a Newly Parameterized LUE Model Based on Crop Water Status and Leaf Chlorophyll Content. *Field Crops Research* **2025**, *333*, 110106, doi:10.1016/j.fcr.2025.110106.
49. Zhang, L.; Niu, Y.; Zhang, H.; Han, W.; Li, G.; Tang, J.; Peng, X. Maize Canopy Temperature Extracted From UAV Thermal and RGB Imagery and Its Application in Water Stress Monitoring. *Front. Plant Sci.* **2019**, *10*, 1270, doi:10.3389/fpls.2019.01270.
50. Reddy, V.R.; Reddy, K.R.; Wang, Z. Cotton Responses to Nitrogen, Carbon Dioxide, and Temperature Interactions. *Soil Science and Plant Nutrition* **1997**, *43*, 1125–1130, doi:10.1080/00380768.1997.11863729.

 doi:10.20944/preprints202604.0463.v1

51. Loka, D.A.; Oosterhuis, D.M.; Ritchie, G.L. Water-Deficit Stress in Cotton. *Stress physiology in cotton* **2011**, *7*, 37–72.
52. Quddus, M.A.; Chowdhury, S.; Jasper, W.; Das, L. Enhancing Cotton Yield Prediction with Robust Deep Neural Network-Based Framework. *European Journal of Agronomy* **2025**, *170*, 127750, doi:10.1016/j.eja.2025.127750.
53. Yoo, C.; Kang, D.; Park, S. Identifying the Impact of Regional Meteorological Parameters on US Crop Yield at Various Spatial Scales Using Remote Sensing Data. *Remote Sensing* **2022**, *14*, 3508, doi:10.3390/rs14153508.
54. Yang, S.; Wang, R.; Zheng, J.; Han, W.; Lu, J.; Zhao, P.; Mao, X.; Fan, H. Remote Sensing-Based Monitoring of Cotton Growth and Its Response to Meteorological Factors. *Sustainability* **2024**, *16*, 3992, doi:10.3390/su16103992.
55. Feng, A.; Zhou, J.; Vories, E.D.; Sudduth, K.A.; Zhang, M. Yield Estimation in Cotton Using UAV-Based Multi-Sensor Imagery. *Biosystems Engineering* **2020**, *193*, 101–114, doi:10.1016/j.biosystemseng.2020.02.014.
56. Hatfield, J.L.; Gitelson, A.A.; Schepers, J.S.; Walthall, C.L. Application of Spectral Remote Sensing for Agronomic Decisions. *Agronomy Journal* **2008**, *100*, S-117-S-131, doi:10.2134/agronj2006.0370c.
57. Camps-Valls, G.; Tuia, D.; Zhu, X.X.; Reichstein, M. Deep Learning for the Earth Sciences: A Comprehensive Approach to Remote Sensing, Climate Science and Geosciences. *Deep Learning for the Earth Sciences: A Comprehensive Approach to Remote Sensing, Climate Science and Geosciences* **2021**, 1–405, doi:10.1002/9781119646181.
58. Molnar, C.; König, G.; Herbinger, J.; Freiesleben, T.; Dandl, S.; Scholbeck, C.A.; Casalicchio, G.; Grosse-Wentrup, M.; Bischl, B. General Pitfalls of Model-Agnostic Interpretation Methods for Machine Learning Models. In *xxAI - Beyond Explainable AI: International Workshop, Held in Conjunction with ICML 2020, July 18, 2020, Vienna, Austria, Revised and Extended Papers*; Holzinger, A., Goebel, R., Fong, R., Moon, T., Müller, K.-R., Samek, W., Eds.; Springer International Publishing: Cham, 2022; pp. 39–68 ISBN 978-3-031-04083-2.
59. Meroni, M.; d'Andrimont, R.; Vrieling, A.; Fasbender, D.; Lemoine, G.; Rembold, F.; Seguini, L.; Verhegghen, A. Comparing Land Surface Phenology of Major European Crops as Derived from SAR and Multispectral Data of Sentinel-1 and -2. *Remote Sensing of Environment* **2021**, *253*, doi:10.1016/j.rse.2020.112232.
60. Zhao, Y.; Jiang, R.; Brider, J.; Chapman, S.; Potgieter, A. Characterizing Wheat and Barley Growth and Phenology Using Multi-Spectral Remote Sensing for Site-Specific Precision Agriculture. in silico *Plants* **2025**, *7*, diaf013, doi:10.1093/insilicoplants/diaf013.